

# Effect of Structural Parameters on the Combustion Performance of Platelet Engines

Yin Liang<sup>1,\*</sup> and Liu Weiqiang<sup>1</sup>

<sup>1</sup>Science and Technology on Scramjet Laboratory, National University of Defense Technology, Changsha, Hunan 410073, People's Republic of China

\*Corresponding e-mail: yl88222@126.com

**Abstract:** Numerical simulation was adopted to determine its flow and combustion characteristics by using gaseous methane and oxygen as the main propellants, the effects of nozzle space and expanding angle are examined for the single element splash platelet injector. Navier-Stokes (*N-S*) equations were solved for the gas-gas flow field with a reduced mechanism involving 9 species and 1 reaction. Results indicated that large corner recirculation zones are produced in the combustor head. This phenomenon consequently enhances mixing and stabilizes combustion, but non-uniformity in temperature contour is observed in the combustor head. Recirculation zone decreases as nozzle space increases, which induces the decrease of maximum temperature and high temperature regions, but it has little influence on the combustion efficiency and combustion length. The combustion length and maximum temperature decrease initially and then increase as expanding angle increases. Conversely, a  $D$  value of 2.4 mm and  $\gamma$  value of  $60^\circ$  are selected for the future works because of the shortest combustion length and minimum temperature of the injector faceplate.

## 1. Introduction

Injector design plays a critical role in the design of a liquid rocket engine. Designed by Aerojet in the 1970s, platelet injector is a new type of liquid rocket injector, which are widely used in low thrust attitude control engine because of their unique features, including excellent response, simple structure, potential high performance with reduced chamber length [1, 2]. The face of a platelet injector is formed from a stack of thin metal platelets which are diffusion bonded into a single unit. The platelet concept was selected because of several features including ease of manufacture and infinite feature geometries with precise tolerance control [3-5], which can provide solutions to difficult thermal and fluid flow problems [6]. Over the past decades, considerable efforts have been dedicated in order to get the baseline performance statistics of platelet injector [7-9].

Boyd [10-13] had an introductory description of the Orbit Maneuvering Engine (OME), followed by a description of the approach chosen for OME uprating, including uprating ground rules and issues. Details values of the current and uprated OME are presented in table 1. The results shown that higher chamber pressure and expansion ratio have significant influences on specific impulse. The injector design used the concept of a platelet injector, the face is formed of twelve photo etched platelets which are bonded together into a 0.088 inch thick stack which is then bonded and welded to the body. Of the 450 elements, 378 are “splash-plate” elements, with 72 “X-doublet” elements in the outer row. Fuel film cooling is provided by 36 “splash-plate” orifices along the outer row.



**Table 1** A comparison of the current and uprated OME

	Current OME	Updated OME
Thrust, lbf	6000	6000
Chamber pressure, psia	125	350
Expansion ratio	55:1	154:1
Mixture ratio	1.65	1.95
Specific impulse, s	315	334
Dry weight, lbm	297	322

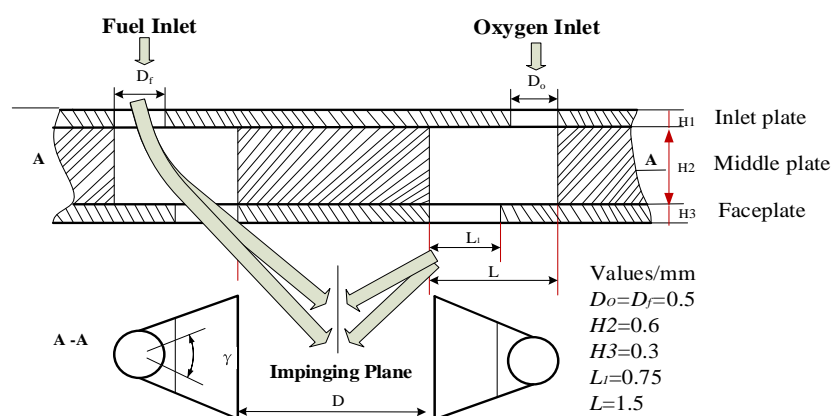
Aerojet Company undertook to evaluate the AJ10-221[13-14] for Orbit Maneuvering Engine in 1985. This engine employs a platelet injector design that includes 92 pre-atomized splash platelet elements. The injector is fabricated from CRES 347 using a photochemical machining and diffusion bonding process. A high-temperature indium/rhenium chamber was also used in these new-generation engines. During the research on AJ10-221, several key technologies are applied:

- (1) A high-temperature indium/rhenium chamber was selected because it provides good low-temperature ductility and high melting point.
- (2) Splash platelet elements were employed for the injector pre-atomized design. The pre-atomized element avoids the problem of requiring perfect alignment/impingement of two small diameter liquid streams for the purpose of propellant atomization.
- (3) The companion technologies for providing metallurgical joints between the different materials used for the injector, chamber, and high area ratio skirt.

This paper presents a numerical analysis of a splash platelet injector using gaseous oxygen and methane as propellants on the ANSYS Fluent platform. In this work, effects of nozzle space ( $D$ ) and expanding angle ( $\gamma$ ) on single element injector are studied. A comparison of combustion flow fields and component distribution are given. This study revealed the baseline performance statistics of a single element injector, which can provide a reference for the structural optimization of the platelet engines.

## 2. Physical method

The schematic of the splash platelet element and its fixed parameters are shown in Figure 1. The key parameters that affect the flow and combustion characteristics include oxidizer orifice ( $D_o$ ), fuel orifice ( $D_f$ ), nozzle space ( $D$ ), expanding angle ( $\gamma$ ), length of trapezoidal orifice ( $L_i$ ), thickness of the middle plate ( $H2$ ), and thickness of the faceplate ( $H3$ ). The design parameters of the chamber thrust are listed in Table 2.

**Figure 1** Schematic of the splash platelet element

**Table 2** Design parameters of the chamber thrust

Parameters	Values
Chamber pressure/MPa	0.85
Mixture ratio(O/F)	3.2
Mass flow rate $m/(g/s)$	44
Gas temperture/K	298.15
Chamber diameter /mm	24.28
Throat diameter /mm	10.86
Theoretical characteristic velocity /(m/s)	1827.3
Ground Specific impulse /(m/s)	2270.2

### 3. Numerical methods

#### 3.1 Governing equations

The three-dimensional, Navier-Stokes and species transport equations for a chemically reacting gas of  $N$  species are given by [15]:

$$\frac{\partial(E - E_v)}{\partial x} + \frac{\partial(F - F_v)}{\partial y} + \frac{\partial(G - G_v)}{\partial z} = H \quad (1)$$

Where  $E$ ,  $F$ ,  $G$  are convective flux vectors

$$E = [\rho u, \rho u u + p, \rho u v, \rho u w, u(\rho e + p), \rho u Y_i]^T \quad (2)$$

$$F = [\rho v, \rho v u, \rho v v + p, \rho v w, v(\rho e + p), \rho v Y_i]^T \quad (3)$$

$$G = [\rho w, \rho w u, \rho w v, \rho w w + p, w(\rho e + p), \rho w Y_i]^T \quad (4)$$

$$H = [0, 0, 0, 0, 0, w_i]^T \quad (5)$$

$$E_v = [0, \tau_{xx}, \tau_{xy}, \tau_{xz}, u\tau_{xx} + v\tau_{xy} + w\tau_{xz} - q_x, \rho_i D_{im} \partial Y_i / \partial x]^T \quad (6)$$

$$F_v = [0, \tau_{yx}, \tau_{yy}, \tau_{yz}, u\tau_{yx} + v\tau_{yy} + w\tau_{yz} - q_y, \rho_i D_{im} \partial Y_i / \partial y]^T \quad (7)$$

$$G_v = [0, \tau_{zx}, \tau_{zy}, \tau_{zz}, u\tau_{zx} + v\tau_{zy} + w\tau_{zz} - q_z, \rho_i D_{im} \partial Y_i / \partial z]^T \quad (8)$$

$$\tau_{xx} = \left[ -\frac{2}{3} \mu \left( \frac{\partial u}{\partial x} + \frac{\partial v}{\partial y} + \frac{\partial w}{\partial z} \right) + 2\mu \frac{\partial u}{\partial x} \right] \quad \tau_{yy} = \left[ -\frac{2}{3} \mu \left( \frac{\partial u}{\partial x} + \frac{\partial v}{\partial y} + \frac{\partial w}{\partial z} \right) + 2\mu \frac{\partial v}{\partial y} \right]$$

$$\tau_{zz} = \left[ -\frac{2}{3} \mu \left( \frac{\partial u}{\partial x} + \frac{\partial v}{\partial y} + \frac{\partial w}{\partial z} \right) + 2\mu \frac{\partial w}{\partial z} \right] \quad \tau_{xy} = \tau_{yx} = \mu \left( \frac{\partial u}{\partial y} + \frac{\partial v}{\partial x} \right)$$

$$\tau_{yz} = \tau_{zy} = \mu \left( \frac{\partial w}{\partial y} + \frac{\partial v}{\partial z} \right) \quad \tau_{xz} = \tau_{zx} = \mu \left( \frac{\partial w}{\partial x} + \frac{\partial u}{\partial z} \right)$$

According to the Fick's law, the following equations can be obtained:

$$\rho_i u_i = \rho D_i \frac{\partial Y_i}{\partial x} \quad (9)$$

$$\rho_i v_i = \rho D_i \frac{\partial Y_i}{\partial y} \quad (10)$$

$$\rho_i w_i = \rho D_i \frac{\partial Y_i}{\partial z} \quad (11)$$

#### 3.2 Turbulence Model

A compressible standard  $\kappa - \varepsilon$  is used for the turbulence model. The turbulence kinetic energy,  $\kappa$ , and its rate of dissipation,  $\varepsilon$ , can be obtained from the following transport equations:

$$\frac{\partial(\rho k)}{\partial t} + \frac{\partial(\rho k u_i)}{\partial x_i} = \frac{\partial}{\partial x_j} \left[ \left( \mu + \frac{\mu_t}{\sigma_k} \right) \frac{\partial k}{\partial x_j} \right] + G_k - \rho \varepsilon \quad (12)$$

$$\frac{\partial(\rho\varepsilon)}{\partial t} + \frac{\partial(\rho\varepsilon u_i)}{\partial x_i} = \frac{\partial}{\partial x_j} \left[ \left( \mu + \frac{\mu_t}{\sigma_\varepsilon} \right) \frac{\partial \varepsilon}{\partial x_j} \right] + C_{1\varepsilon} \frac{\varepsilon}{k} G_k - C_{2\varepsilon} \rho \frac{\varepsilon^2}{k} \quad (13)$$

The turbulent viscosity,  $\mu_t$ , can be computed by combining  $\kappa$  and  $\varepsilon$  as follows:

$$\mu_t = \rho C_\mu \frac{\kappa^2}{\varepsilon} \quad (14)$$

Where,  $C_{1\varepsilon} = 1.44$ ,  $C_{2\varepsilon} = 1.44$ ,  $C_\mu = 0.09$ ,  $\sigma_\kappa = 1.0$ ,  $\sigma_\varepsilon = 1.3$

### 3.3 Boundary condition

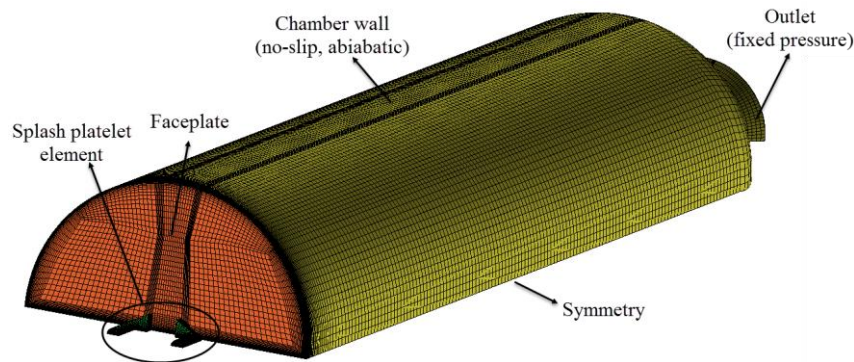
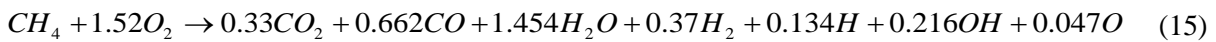


**Figure 2** Grid of the calculation domain

Figure 2 shows the grid of the calculation domain and boundary condition. A symmetry boundary condition was adopted for the single element injector. For the boundary conditions, the inlets of methane and oxygen are characterized by a fixed mass flow rate, and the inlet turbulence intensity is set at 5%. The inlet temperatures of methane and oxygen are set at 298.15 K. The nozzle exit is specified as a supersonic outlet, and adiabatic nonslip wall boundaries are enforced at chamber walls [16, 17]. In the solution method, the coupling scheme with second order upwind discretization for all transported scalars is used.

### 3.4 Chemical kinetics mechanism

Navier-Stokes equations and the standard  $\kappa$ - $\varepsilon$  turbulence model are used to calculate the combustion flow field of the combustor. In the present simulations, a detailed  $\text{O}_2/\text{CH}_4$  chemical kinetics mechanism involves dozens of chemical species with hundreds of elementary reactions. A reduced mechanism, which contains 9 species and 1 reaction, is utilized in this study to save computing time. The interaction between turbulence and reaction was considered by the EDC model [18, 19].



## 4. Result and Discussion

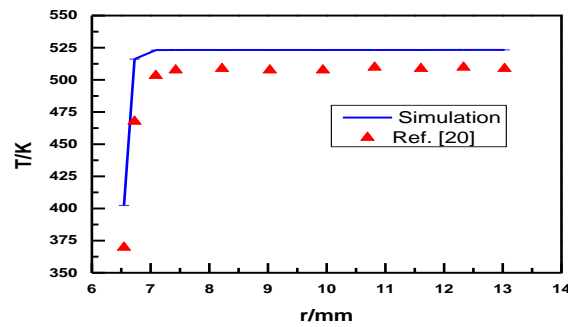
### 4.1 Validation of numerical methods

**Table 3.** Design parameters of the shear-coaxial injector

Propellant	$m/(\text{g/s})$	$MR$	$P_c/\text{MPa}$	$D_c/\text{mm}$	$D_f/\text{mm}$	$L^*/\text{mm}$	$R_v$
GCH <sub>4</sub> /GO <sub>2</sub>	5.5	3.5	3	26	14.8	1180	1.77

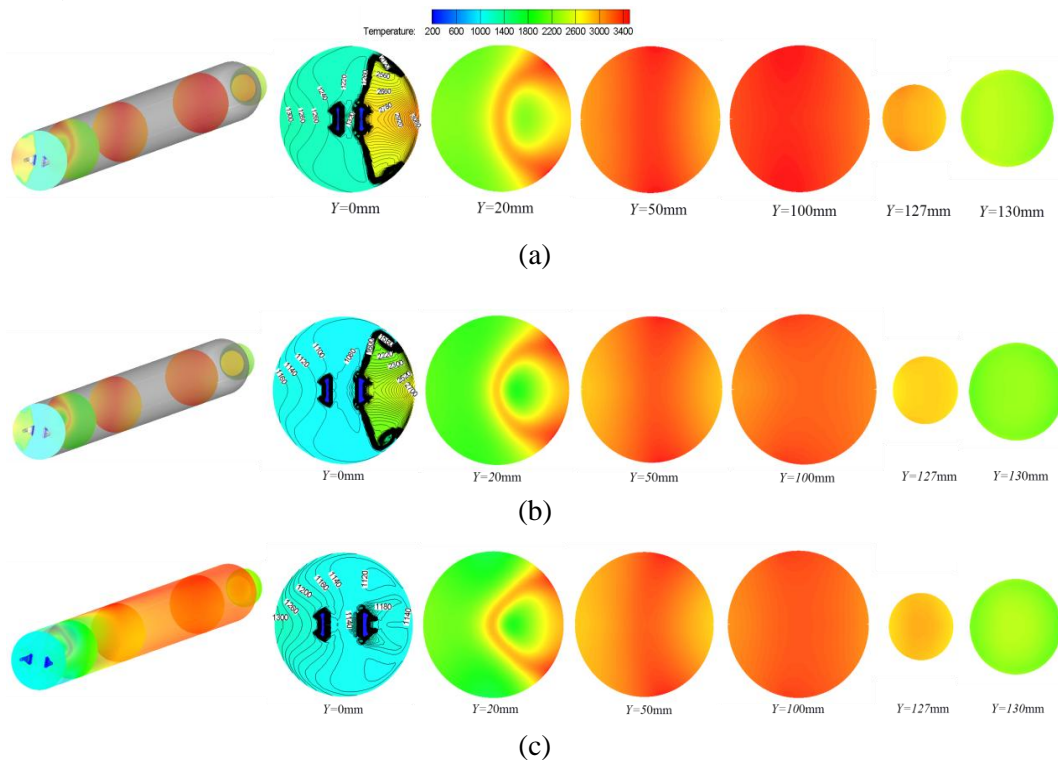
To demonstrate the validity of numerical methods and chemical kinetics model, simulation was performed on a shear-coaxial GO<sub>2</sub>/GCH<sub>4</sub> injector, where  $P_c$  is the chamber pressure,  $MR$  is mixture

ratio,  $D_c$  is chamber diameter,  $D_t$  is throat diameter,  $L^*$  is the characteristic length,  $R_v$  is the velocity ratio. The parameters of the shear-coaxial injector are listed in Table 3, and the detail design values can get from Ref.[20]. Figure 3 shows the temperature distribution of the oxidizer post, which is consistent with the Ref. data; it can exactly describe the temperature distribution although there is little difference. This testified the accuracy of numerical methods and chemical kinetics model. Detailed chemical reaction model should be adopted in the future works.

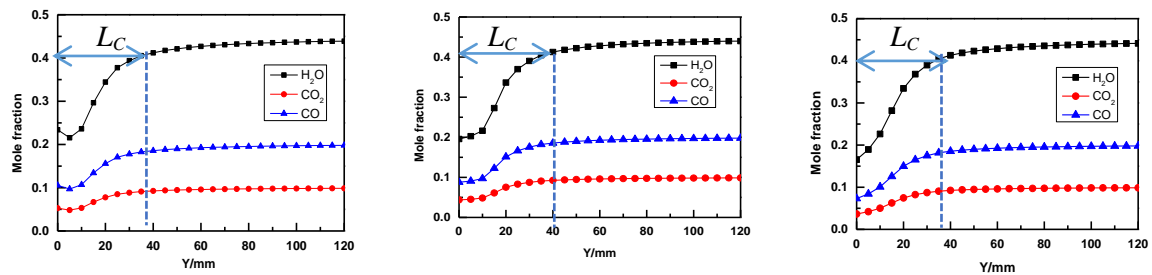


**Figure 3.** Temperature distribution of the oxidizer post

#### 4.2 Effect of $D$ on the combustion characteristics



**Figure 4** Temperature distributions for different nozzle spaces: (a)  $D=1.2\text{mm}$ ; (b)  $D=1.8\text{mm}$ ; and (c)  $D=2.4\text{mm}$

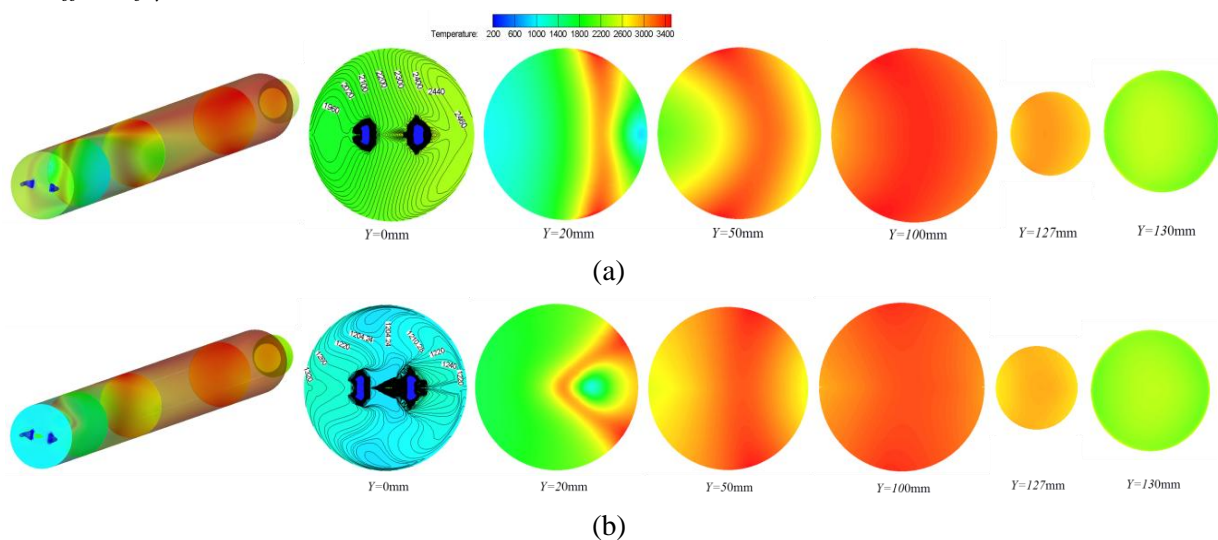
(a)  $D = 1.2$  mm(b)  $D = 1.8$  mm(c)  $D = 2.4$  mm**Figure 5** Effect of nozzle spaces on  $\text{H}_2\text{O}$ ,  $\text{CO}_2$  and  $\text{CO}$  mole fraction

When studying the effect of nozzle space  $D$ , expanding angle  $\gamma$  is fixed as 60 degree. Figure 4 shows the average temperature distribution in the cross section. As calculated in the simulation, the combustor temperature is as high as 3400 K, which is similar to the theoretical value.  $D$  has significantly influences on the temperature in the chamber head. As  $D$  increase, the recirculation zones on the front part of the combustor and gas temperature decrease. These recirculation zones appear mainly at the position of  $Y = [0, 30 \text{ mm}]$  away from the injector faceplate, which induces mixing enhancement and combustion stability. The influence of recirculation zones decrease with the development of the combustion process, which leads to more well-distributed temperature in the combustor.

For methane combustion, the proportion of water is larger than that of other components. Therefore, the main combustion area and combustion length can be revealed by analysing the mole fraction of water. In this study, the combustion length is defined as  $L_c$  when the mole fraction of water is 90% of the theoretical value.

The effect of  $D$  on  $\text{CO}_2$ ,  $\text{CO}$ ,  $\text{H}_2\text{O}$  mole fraction is shown in Figure 5. As  $D$  increase, the mole fractions increase rapidly and then reach a balance in a shorter combustion length. The  $\text{CO}_2$ ,  $\text{CO}$ ,  $\text{H}_2\text{O}$  mole fraction make slightly differ with  $D = 1.2, 1.8$ , and  $2.4 \text{ mm}$ . When  $D = 2.4 \text{ mm}$ , the corresponding combustion length is about  $40 \text{ mm}$ .

#### 4.3 Effect of $\gamma$ on the combustion characteristics





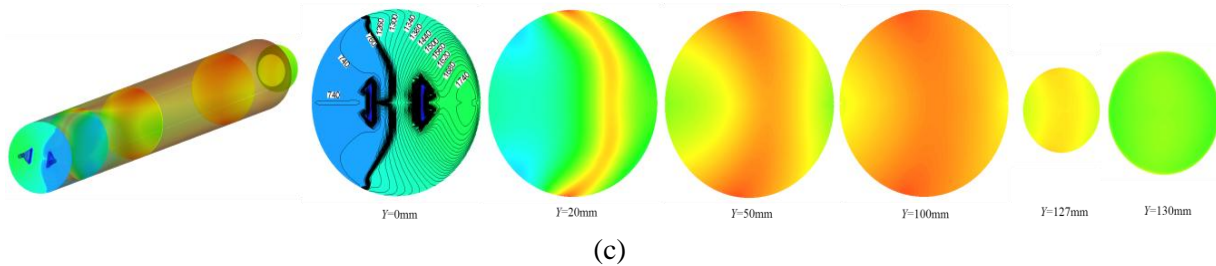


**Figure 6** Temperature distributions for different expanding angles: (a)  $\gamma = 30^\circ$ ; (b)  $\gamma = 45^\circ$ ; and (c)  $\gamma = 75^\circ$

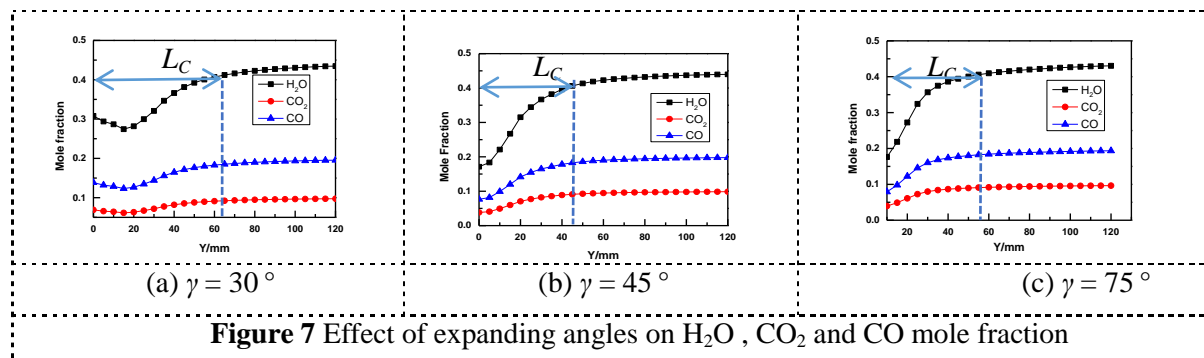


**Figure 7** Effect of expanding angles on  $\text{H}_2\text{O}$ ,  $\text{CO}_2$  and  $\text{CO}$  mole fraction

When studying the effect of expanding angle  $\gamma$ , nozzle space  $D$  is fixed as 2.4mm. In the follow-up study,  $\gamma$  is selected as a decision variable, where  $\gamma=30, 45$ , and  $75$  degree. As  $\gamma$  increases, the flow area increases, but the velocity ratio remains the same. Figure 6 shows the temperature distributions for different expanding angle. Non-uniform Temperature is found in the combustion chamber head because of the characteristics of the splash platelet element. Compared with the effect of  $D$ , expanding angle has greater influence on the temperature distributions in the combustor head.

The effect of  $\gamma$  on the  $\text{CO}_2$ ,  $\text{CO}$ ,  $\text{H}_2\text{O}$  mole fraction is shown in Figure 7. Results show that the combustion length initially decreases and then increase as  $\gamma$  increase. The mole fraction of  $\text{H}_2\text{O}$  is quite different in the combustion chamber head, the combustion length are 76mm, 55mm, 62mm, respectively. A comparison with the above results shows that when  $\gamma=60^\circ$ , the combustion length is the shortest.

#### 4.4 Temperature of the injector faceplate

Aerodynamic heating remarkably affects the reliability of injector faceplates. The effect of the aerodynamic heating of platelet injector can be more severe than those of traditional injector because of several unique features, such as shorter chamber length and thinner faceplate. A large-corner recirculation zone produced in the combustion chamber head because of the characteristics of the splash platelet element, which induces mixing enhancement and combustion stability but creates a heat flux peak on the injector faceplate. Figure 4 and 6 ( $Y=0\text{mm}$ ) shows the temperature distributions of injector faceplate. The results show that the high temperature region and the maximum temperature decrease as  $D$  increase. When  $D=1.2\text{mm}$ , the maximum temperature can be 3000 K, which exceeds the limit value of 1Cr18Ni9Ti ( $T<1400\text{K}$ ). The maximum temperature initially decreases and then increases as  $\gamma$  increase. When  $\gamma=45^\circ$ , the maximum temperature is not exceeding 1400K. In all of the simulations, the temperatures of the injector faceplates exceed their limit. Therefore, faceplates with cooling techniques should be designed.

## 5. Conclusions

The combustion characteristics of a single element splash platelet injector with  $\text{GO}_2/\text{GCH}_4$  as propellant were discussed through CFD simulation, and the effects of  $D$  and  $\gamma$  were examined. The following conclusions can be obtained:

- (1) As  $D$  increase, the recirculation zones on the front part of the combustor and gas temperature decrease. Nozzle space has significant influences on the flow field in the combustor head, but it has little influences on the composition distribution and combustion length.
- (2) As  $\gamma$  increase, the flow area increase, but the velocity ratio remains the same. Non-uniform temperature is found in the combustion chamber head, which has significant influence on the combustion length, the combustion length initially decreases and then increase as  $\gamma$  increase.
- (3) The high temperature region and the maximum temperature decrease as  $D$  increase, and the maximum temperature initially decreases and then increases as  $\gamma$  increase. In all of the simulations, the temperatures of the injector faceplates nearly exceed their limit. Therefore, faceplates with cooling techniques should be designed.

### Acknowledgment

This work is supported by National Science Foundation of China (Grant NO. 90916018) and Hunan Provincial Natural Science Foundation (Grant NO. 13JJ2002)

### References

- [1] H. H Mueggengurg. Platelet injector design and development history. AIAA/SAE/ASME/ASEE 27th Joint Propulsion Cong, 1991.
- [2] KahL R C, Labotz R J, Bassham L B. Platelet Injector for Space Shuttle Orbital Maneuvering Engine, AIAA/SAE 10th Propulsion Cong, 1974.
- [3] Liu W Q, Sun J, Nie T, et al. A structure of platelet heat-pipe-cooled leading edge, China Patent, ZL201310311505.5[P]. 2013-12-04.
- [4] S.A. Poniaev, R.O. Kurakin, A.I. Sedov, et al. Hypervelocity impact of mm-size plastic projectile on thin aluminum plate Original Research Article, *Acta Astronautica*, 135(2017):26-33.
- [5] Liu H P, Liu W Q. A numerical model for the platelet heat-pipe-cooled leading edge of hypersonic vehicle, *Acta Astronautica*, 118(2016) : 210-217.
- [6] B. A. Robbers, B. J. Anderson, W. A. Hayes, et al. Platelet devices-limited only by one' s imagination, 42nd AIAA/ASME/SAE/ASEE Joint Propulsion Conference & Exhibit 9-12 July 2006, Sacramento, California.
- [7] Donald M J, Sanders D R, Leonard S. Durability Testing of the AJ10-221 490N High performance (321 Sec Isp) Engine, AIAA/SAE/ASME/ASEE 29th Joint Propulsion Conference and Exhibit, June 28-30, 1993, Monterey, CA.
- [8] Sanders D R, Leonard S. New generation of high-performance engines for spacecraft propulsion, *Journal of Propulsion and Power*, Vol.10, No. 1, Jan.-Feb. 1944.
- [9] D. David. Space Shuttle Maneuvering Subsystem (OMS) Rocket Engine Development Status Update July 1977, AIAA/SAE 13th Propulsion Conference, July 11-13, 1977, Orlando, Florida.
- [10] Boyd, W, and Mallini C. Shuttle Performance Enhancement Using An Upated OMS Engine, AIAA/ASME/SAE/ASEE Joint Propulsion Conference Boston, Massachusetts, July, 1988
- [11] J. D. Bertolino, W. C. Boyd. Upated OMS Engine Status-Sea Level Testing Results, N91-24256.
- [12] Boyd, W., and Brasher, W. Upated OMS Engine Status and Future Applications, AIAA/ASME/SAE/ASEE 22nd Joint Propulsion Conference, Huntsville, Alabama, June, 1986.
- [13] Rosenberg, S. D., and Schoenman, L. New Generation of High Performance Engines for Spacecraft Propulsion, *Journal of Propulsion and Power*, 10(1): 40-46, 1994.
- [14] Schoenman, L, Rosenberg, S. D., and Jassowski, D. M. Test Experience, 490-N High performance [321-s Specific Impulse] Engine, *Journal of Propulsion and Power*, 11(5): 992-997, 1995.



- [15] Jin, P, Xu X, and Cai G B, Numerical simulation of combustion chamber of FFSC with gas-gas injectors [C], IAC-05-C4.P.18, 56th International Astronautical Congress, Oct 17-21, 2005, Fukuoka, Japan.
- [16] Wang X W, Cai G B, Jin P. Scaling of the flowfield in a combustion chamber with a gas-gas injector, *Chin. Phys. B*, 19(1), 019401, 2010.
- [17] Conley A, Vaidyanathan A, Segal C, Heat flux measurements for a  $\text{GO}_2/\text{GH}_2$  single-element, shear injector, *Journal of Spacecraft and Rockets*, 44(3): 633-639, 2007.
- [18] Sozer E, Vaidyanathan A, Segal C, et al, Computational assessment of gaseous reacting flows in single element injector, AIAA Paper No.2009-449.
- [19] N. Ierardo, A. Congiunti, C. Bruno, Mixing and Combustion in Supercritical  $\text{O}_2/\text{CH}_4$  Liquid Rocket Injectors, 42th AIAA Aerospace Sciences Meeting and Exhibit, January 5-8, Reno, Nevada, 2004.
- [20] Gao Yushan, Du Zhenggang, Jin Ping, Cai Guobiao, Numerical simulation on the combustion characteristic of shear coaxial  $\text{GO}_2/\text{GCH}_4$  injector, *Journal of rocket propulsion*, 35(5): 18-23, 2009.